Conformational ensemble of a multidomain protein explored by Gd^{3+} electron paramagnetic resonance

Tomohide Saio,[1†]* Soya Hiramatsu,[2†] Mizue Asada,[3] Hiroshi Nakagawa,[4,5] Kazumi Shimizu,[6] Hiroyuki Kumeta,[7] Toshikazu Nakamura,[3] and Koichiro Ishimori[2,8] *

[1]*Division of Molecular Life Science, Institute of Advanced Medical Sciences, Tokushima University, Tokushima, Japan*

[2]*Graduate School of Chemical Sciences and Engineering, Hokkaido University, Sapporo, 060-8628, Japan*

[3]*Instrument Center, Institute for Molecular Science, Okazaki 444-8585, Japan.*

[4]*Materials Sciences Research Center, Japan Atomic Energy Agency, Tokai, Ibaraki 319-1195, Japan*

[5] *J-PARC Center, Japan Atomic Energy Agency, Tokai, Ibaraki 319-1195, Japan*

[6] *Faculty of Education and Integrated Arts and Sciences, Waseda University, Tokyo 169-8050, Japan*

[7] *Faculty of Advanced Life Science, Hokkaido University, Sapporo, 011-0021, Japan*

[8]*Department of Chemistry, Faculty of Science, Hokkaido University, Sapporo, 060-0810, Japan*

[†]These authors contributed equally to this work.

*Corresponding author E-mail: saio@tokushima-u.ac.jp, koichiro@sci.hokudai.ac.jp

Running title: Structural variation of a protein enzyme

Keywords: Conformational ensemble, integrated structural analysis, DEER EPR, NMR, lanthanide ion

ABSTRACT

Despite their importance in function, the conformational state of proteins and its changes are often poorly understood mainly because of the lack of an efficient tool. MurD, a 47-kDa protein enzyme responsible for peptidoglycan biosynthesis, is one of those proteins whose conformational states and changes during their catalytic cycle are not well understood. Although it has been considered that MurD takes a single conformational state in solution as shown by a crystal structure, the solution NMR study suggested the existence of multiple conformational state of apo MurD in solution. However, the conformational distribution has not been evaluated. In this work we investigate the conformational states of MurD by the use of electron paramagnetic resonance (EPR), especially inter-gadolinium distance measurement using double electron–electron resonance (DEER) measurement. The gadolinium ions are fixed on specific positions on MurD via a rigid double-arm paramagnetic lanthanide tag that has been originally developed for paramagnetic nuclear magnetic resonance (NMR). The combined use of NMR and EPR enables accurate interpretation of the DEER distance information to the structural information of MurD. The DEER distance measurement for apo MurD shows a broad distance distribution, whereas the presence of the inhibitor narrows the distance distribution. The results suggest that MurD exists in a wide variety of conformational states in the absence of ligands, whereas binding of the inhibitor eliminates variation in conformational states. The multiple conformational states of MurD were previously implied by NMR experiments, but our DEER data provided structural characterization of the conformational variety of MurD.

STATEMENT OF SIGNIFICANCE (<120)

A rigid double-arm lanthanide tag was utilized in electron paramagnetic resonance spectroscopy to measure the distance between two specific points on a protein enzyme MurD, and the conformational states and distribution of MurD were investigated. Although previous crystallographic and NMR studies have reported the three distinct conformational states of MurD, our data showed that the protein exists in a much wider variety of conformational states

in the absence of ligands. Given the fact that MurD is one of the potent drug targets for infectious diseases, it is projected that the findings in this study will provide an important structural basis for drug development.

INTRODUCTION

Proteins, especially protein enzymes, exert their activities through dynamic structural changes that are often poorly understood. Even after the determination of their high-resolution structure, the lack of information about these dynamic structural changes obscures the understanding of the mechanism. MurD, a 47-kDa protein enzyme responsible for peptidoglycan biosynthesis, is one of those proteins whose conformational states and changes are critical for regulating its catalytic process (1). MurD is a member of Mur ligase family that is responsible for peptidoglycan biosynthesis, and catalyzes the ligation of D-Glu to UDP-*N*-acetylmuramoyl-L-alanine (UMA) coupled with adenosine triphosphate (ATP) hydrolysis, in which ATP, UMA, and D-Glu need to bind sequentially to MurD (2). Given the high stereospecificity toward D-Glu (3) and conserved D-Glu-binding site across different bacterial species (4), MurD has been extensively studied as a potent drug target among the Mur ligases (5, 6, 7).

MurD consists of three domains, and previous crystallographic studies have identified that domain 3 undergoes drastic orientational changes with respect to domain 2, so that MurD changes its conformation from the open to the closed state upon binding to ligands or inhibitors (1, 2, 5, 6, 8, 9). More recently, a nuclear magnetic resonance (NMR) study using paramagnetic lanthanide ions showed that drastic conformational changes of MurD regulate the order of the ligand binding in the enzymatic reaction (10). Interestingly, the NMR study also suggested that MurD exists in multiple conformational states exchanging in millisecond to microsecond (ms–μs) time scale in the absence of ligands (10), whereas it had been believed that apo MurD exists in the open conformation as seen in the crystal structure (10). However, these conformational variations of MurD are not fully understood. The conformational equilibrium can be hindered upon crystal formation, or in the solution NMR experiments, the conformational exchange averages or broadens out the resonances, which obscures the structural information for each of the states. Molecular dynamics (MD) simulations have been performed to investigate the conformational dynamics of MurD *in silico* (11, 12), but limited simulation time has, so far, impeded the tracking of the relatively large size as well as slow conformational dynamics (ms–μs

time scale) of MurD.

In this study, to obtain information about the conformational ensemble of MurD, we used electron paramagnetic resonance (EPR) utilizing double electron–electron resonance (DEER). DEER distance measurement provides nanometer-scale distance and population for the paramagnetic centers introduced at specific positions of the protein, and thus potentially resolves the multiple conformational states in the equilibrium (13-16). Gd^{3+} ion as a paramagnetic center can be introduced to the protein using lanthanide-binding tags (17, 18). Among several paramagnetic centers, including nitroxide spin label (19) and copper ion (20), one of the advantages of Gd^{3+} ion in DEER is availability of plenty of lanthanide-binding tags that have been extensively developed originally for use in protein NMR (17, 18). Especially, the availability of the double-arm tag is advantageous because the double-arm tags reduce the mobility of the tag with respect to the protein (21-23), and are thus expected to provide higher resolution of structural information. The advantages of double-arm tags have been initially demonstrated in the field of paramagnetic NMR (17, 18), but more recently in DEER measurements in EPR as well (24). In this study we use the double-armed lanthanide tag, Caged Lanthanide NMR Probe 5 (CLaNP-5) (21, 25), which is one of the most extensively used tags in protein NMR experiments (10, 26-28) but has not been used in the DEER distance measurement. We here demonstrate the use of CLaNP-5 tag in DEER EPR for accurate nanometer-scale distance measurements.

The EPR data show that MurD in the absence of the ligand exists as an ensemble of multiple conformational states, whereas the ligand binding induces a drastic conformational change that focuses the conformational ensemble toward the closed state. Well-defined metal positions with respect to MurD domains owing to the PCS-NMR analysis as well as the rigid architecture of the CLaNP-5 tag enabled us to obtain detailed structural information on MurD in the absence and presence of the inhibitor. Our data indicate that MurD can take a much larger number of conformational states than previously thought on the basis of crystallographic and NMR studies (1, 2, 5, 8-10, 29). Given the usefulness of the CLaNP-5 tag in protein NMR study,

it was expected that application of the tag in EPR will further accelerate the combined use of EPR and paramagnetic NMR in protein structural and dynamics study.

MATERIALS AND METHODS

Preparation of CLaNP-5

CLaNP-5 was synthesized, purified, and chelated to Lu^{3+}, Yb^{3+}, and Gd^{3+} according to the procedure described in previous reports (10, 21, 25).

Protein sample preparation

Escherichia coli MurD full-length (1–437), domain 1–2 (1–302), and domain 3 (301–437) were cloned into pGBHPS (30), expressed in *E. coli* strain BL21 (DE3), and purified as described in a previous report (10). For PCS observation, isotopically labeled MurD domain 1–2 Q170C/V172C ($D12_{170}$) and MurD domain 1–2 M145C/D148C/C151A ($D12_{145}$), both having a single lanthanide ion, were prepared using the same procedure as reported previously for MurD domain 1–2 E260C/K262C (10). The proteins were prepared in a buffer containing 20 mM Tris–HCl (pH 7.2) and 100 mM NaCl. The CLaNP-5 tag was attached to the protein by mixing the protein and the tag at a 1:1.1 ratio for 15 minutes on ice, followed by gel filtration to remove unreacted tag. For EPR distance measurement, MurD domain 1–2 Q170C/V172C/E260C/K262C ($D12_{170–260}$), MurD domain 1–2 M145C/D148C/C151A/E260C/K262C ($D12_{145–260}$), and MurD E260C/K262C/N360C/D362C ($MurD_{260–360}$) were prepared using a previously described procedure (10). Note that $D12_{145–260}$ has a mutation in C151A aiming to avoid intramolecular disulfide bond formation with D148C. The CLaNP-5 tag was attached to the protein by mixing the protein and the tag at a 1:2.2 ratio for 15 minutes on ice, followed by gel filtration. The attachment of the tag was confirmed by NMR (Figure S1–S2). The data showed that the tags were attached to the specific position of MurD at a high efficiency. Although MurD has seven cysteine residues (C20, C99, C151, C208, C227, C368, and C413), all cysteine residues have a thiol group buried in the protein and did not react to the CLaNP-5 tag (10). MurD domain 1–2 Q170C/V172C/E260C/K262C ($D12_{170–260}$) was prepared in 20 mM Tris-d_{11}-HCl (pD 7.2), 100 mM NaCl in 70% D_2O/30% glycerol-d_8. Full-length MurD E260C/K262C/N360C/D362C

(MurD$_{260–360}$) and full-length MurD E260C/K262C/L396C/R400C (MurD$_{260–396}$) were prepared in 20 mM Tris-d_{11}-HCl (pD 7.2), 200 mM NaCl in 70% D_2O/30% glycerol-d_8.

Determination of the metal position by PCS analysis

The positions of the metal fixed at Q170C/V172C and M145C/D148C were estimated via analysis of PCSs (31, 32). The diamagnetic lanthanide ion Lu^{3+} as a diamagnetic reference or the paramagnetic lanthanide ion Yb^{3+} was attached to MurD domain 1–2 Q170C/V172C (D12$_{170}$) or MurD domain 1–2 M145C/D148C/C151A (D12$_{145}$) by CLaNP-5. PCSs were measured as a chemical shift difference between the backbone amide resonances from paramagnetic and diamagnetic samples. To reduce the number of resonances in the spectra for more reliable PCS assignments, amino acid-selective ^{15}N-labeled samples were prepared as previously described (10). ^{1}H–^{15}N heteronuclear single quantum coherence (HSQC) spectra were recorded on Bruker Avance III 600 and 800 MHz NMR spectrometers (Bruker Corp., Billerica, MA, USA). The spectra were recorded at 25°C. Spectra were then processed using the NMRPipe program (33), and data analysis was performed on the Olivia program (Yokochi et al.; https://github.com/yokochi47/Olivia). Δχ-tensor and the position of the lanthanide ion were calculated from the PCS values and the crystal structure of MurD (PDB code 3uag) (2), using the Numbat program (34) with equation Eq. (1),

$$\Delta\delta^{\mathrm{PCS}} = \frac{1}{12\pi r^3}\left[\Delta\chi_{\mathrm{ax}}(3\cos^2\theta - 1) + \frac{3}{2}\Delta\chi_{\mathrm{rh}}\sin^2\theta\cos 2\phi\right], \quad (1)$$

where $\Delta\delta^{\mathrm{PCS}}$ is the PCS; r, θ, and φ are the polar coordinates of the nucleus with respect to the principal axes of the magnetic susceptibility tensor; and $\Delta\chi_{ax}$ and $\Delta\chi_{rh}$ are the axial and rhombic components, respectively, of the anisotropic magnetic susceptibility tensor. The tensor calculations were performed using 63 and 31 PCSs induced by Yb^{3+} and Tm^{3+}, respectively, for D12$_{145}$ (Table S1) and using 87 PCSs induced by Yb^{3+} for D12$_{170}$ (Table S2). Only PCSs observed from the amide proton located on the rigid region of the protein were used in the fitting.

Errors were estimated with Monte Carlo analysis using the 100 partial PCS data sets in which 30% of the input data were randomly deleted.

Determination of the metal position by modeling

The position of the metal fixed via N360C/D362C was estimated by docking calculation using Xplor-NIH (35). The coordinates of CLaNP-5 were prepared as described previously (31, 36), by using PRODRG2 server (37) and VEGA ZZ (38). In the Xplor calculation, the position and orientation of CLaNP-5 were first randomized around the coordinate of MurD (PDB ID: 3uag) and then docked onto MurD with distance restraints between the sulfur atoms in the double arm of CLaNP-5 and cysteine residues at N360 and D362 of MurD. A total of 100 docking calculations were performed, and the 50 lowest-energy coordinates were selected, in which the positions of the metal were averaged.

EPR DEER distance measurement

EPR spectra were recorded using a Bruker E680 spectrometer (Bruker Corp.). All EPR signals were detected at 10 K with a CF935 liquid helium cryostat (Oxford Instruments, Oxford, UK) using Q band (34.2 GHz). For echo-detected (ED) EPR measurement, we used a π/2–τ–π sequence with a time interval τ of 200 ns with pulse lengths of 16 and 32 ns. Repetition time was 500 μs. For DEER measurement, a four-pulse sequence $\pi/2(\nu_{obs})–\tau_1–\pi(\nu_{obs})–t–\pi(\nu_{pump})–(\tau_1 + \tau_2 - t)–\pi(\nu_{obs})–\tau_2–echo$ with a time interval τ_1 of 400 ns and τ_2 of 4000 ns were used. Pulse lengths of the observation π/2 and π pulse were 16 and 32 ns, respectively, and the length of the pumping pulse was 20 ns. Repetition time was 500 μs. Artifact signals arising from multiple pulses were removed using an eight-step phase cycling. The microwave frequencies for observation and pumping pulses for DEER with a difference of 100 MHz were set to resonate with the magnetic fields indicated by arrows in Figure S4. The distance distributions were estimated using

DeerAnalysis 2016 software (39).

RESULTS

Gadolinium tagging of a multidomain protein MurD

To investigate the conformational states of a multidomain protein MurD, we aimed to measure the distance between the two gadolinium ions fixed on the domains 2 and 3 by DEER experiments. Gd^{3+} ion was fixed on MurD through the CLaNP-5 tag (21, 25) that was attached to the protein by two disulfide bridges (Figure 1). For reliable DEER distance measurements, the tagging points were designed to be located within ~8 nm from each other and located on the structured region of MurD, with the reference of the crystal structure of MurD (PDB ID: 3uag) (2). The amino acid residues located on the long loop or disordered regions were excluded from the candidates. Finally, four positions of MurD—three in domain 2 and one in domain 3—were selected for gadolinium tagging (Figure 1a–c). Following the procedures described in previous reports (10, 25), the pair of surface-exposed residues whose C_β atoms are located in a distance of 8–10 Å were selected and mutated to cysteine residues for attachment of CLaNP-5 (Figure 1e). Three MurD variants were constructed for DEER measurement: MurD domain 1–2 M145C/D148C/C151A/E260C/K262C ($D12_{145–260}$), MurD domain 1–2 Q170C/V172C/E260C/K262C ($D12_{170–260}$), and full-length MurD E260C/K262C/N360C/D362C ($MurD_{260–360}$) (Figure 1a–c). Because $D12_{145–260}$ and $D12_{170–260}$ have two Gd^{3+} ions both on domain 2, the distance distributions for $D12_{145–260}$ and $D12_{170–260}$ are expected to reflect local conformational variation around the tag. On the other hand, the distance distribution for $MurD_{260–360}$, having Gd^{3+} ions on domains 2 and 3, is expected to reflect the conformational variations of domain 3 with respect to domain 2, in addition to the local conformational variations.

Determination of metal positions with respect to MurD domains

Before the DEER experiments, the positions of each of the metal ions with respect to the domain holding the CLaNP-5 tag were determined. The precise metal positions with respect to the domains enables the interpretation of the DEER distance data to the detailed structural information of MurD. The position of the metal fixed at E260C/K262C was previously determined by PCSs observed by NMR (10), whereas the positions of the metal fixed at M145C/D148C and Q170C/V172C were determined by PCSs in this study. For PCS measurements, instead of Gd^{3+}, an anisotropic paramagnetic lanthanide ion Yb^{3+} or diamagnetic lanthanide ion Lu^{3+} was attached to MurD domain 1–2 M145C/D148C/C151A ($D12_{145}$) and MurD domain 1–2 Q170C/V172C ($D12_{170}$) by CLaNP-5, and the PCSs were observed as chemical shift differences between paramagnetic and diamagnetic resonances (Figures S1 and S2). Significant PCSs were observed from the resonances of the amide groups (Tables S1 and S2). The parameters of the anisotropic magnetic susceptibility tensor ($\Delta\chi$-tensor), including the metal position, were determined using Numbat program (34) (Table 1 and Figure S3). The values of $\Delta\chi_{ax}$ and $\Delta\chi_{rh}$ are close to those determined for Yb^{3+} attached at another position of MurD, at E260C/K262C (10), and to another protein (25). Furthermore, the position of the lanthanide ion was well defined, indicating that the tag was rigidly fixed on MurD. Given the position of the metal fixed via E260C/K262C that was previously determined with the same procedure using the same coordinates of MurD (PDB code: 3uag) (10), the distances between the lanthanide ions fixed at the two positions, M145C/D148C and E260C/K262C, and Q170C/V172C and E260C/K262C, were estimated as 3.58 ± 0.12 and 3.86 ± 0.11 nm, respectively (Figure 1a and b). The metal position for N360C/D362C was estimated by docking calculation using Xplo-NIH (35) (Figure 1e), because of the limited solubility of the isolated MurD domain 3 N360C/D362C (see Materials and methods).

Gd^{3+}–Gd^{3+} DEER measurement for $D12_{145–260}$ and $D12_{170–260}$

The distance distribution obtained from DEER measurement should provide information about the conformational variety of the protein given that the different

conformational states of the protein have distinct distances between paramagnetic centers. However, it should be noted that the residual mobility of the tag can also contribute to the distance distribution. Although the CLaNP-5 tag is rigidly attached to the protein via two arms as shown by previous NMR studies (10, 21, 25), there was no information about the actual spatial distribution of the metal ion attached on the protein via CLaNP-5 tag. To assess the distribution of paramagnetic centers imposed by the residual local mobility of the CLaNP-5 tag, we performed DEER measurement on $D12_{145–260}$ and $D12_{170–260}$, in which CLaNP-5 tags containing Gd^{3+} were attached to the rigid regions of domain 2 (Figure 1a and b). The EPR experiments were performed on $D12_{145–260}$ and $D12_{170–260}$ prepared in 80% ^2H_2O/20% glycerol-d_8 solution at 10 K on a Q-band spectrometer (resonant frequency, 34 Hz) (Figure S4). The central transition peak in the ED EPR spectrum was similar to the previously reported data recorded on a Q-band spectrometer (resonant frequency, 34 Hz) (40). Four-pulse DEER experiments were performed on $D12_{145–260}$ and $D12_{170–260}$, and distance distributions were obtained using DeerAnalysis 2016 (39) (Figure 2). The data were recorded with dipolar evolution time as long as 3.9 μs. The DEER trace exhibited clear dipolar modulation (Figure 2a–d), indicating the existence of the defined inter-metal distance. Tikhonov regularization and Gaussian fit for $D12_{145–260}$ showed the most intense peaks at 3.64 and 3.68 nm, with full-width at half-maximum (FWHM) of 0.77 and 0.76 nm, respectively (Figure 2e). The fitting for $D12_{170–260}$ showed the most intense peaks at 3.96 nm (Tikhonov regularization) and 3.90 nm (Gaussian fit), with FWHM of 0.75 and 0.67 nm, respectively (Figure 2f). In both cases, Tikhonov regularization and Gaussian fit showed essentially the same distance distribution, supporting the robustness of the analysis. Thus, FWHM of 0.7-0.8 nm are considered to be imposed by local conformational variations of the lanthanide tag. Assuming that the two CLaNP-5 tags have similar conformational distributions, the DEER distance distribution indicated that each CLaNP-5 tag has conformational distribution of 0.4 nm, which should be mainly accounted for local conformational variation of side chains of the cysteine residues holding the tag. These DEER-derived distances match the distances estimated by $\Delta\chi$ tensor analysis using PCSs and the crystal structure of MurD, 3.58 ± 0.12 nm for $D12_{145–260}$, and 3.86 ± 0.11 nm for $D12_{170–260}$ (Figure 1a and b), supporting the reliability of

the Gd^{3+}–Gd^{3+} distance measurement by DEER.

Gd^{3+}–Gd^{3+} DEER for $MurD_{260–360}$ identified a variety of conformational states of MurD

The Gd^{3+}–Gd^{3+} distance for $MurD_{260–360}$ was measured to monitor the conformational states of MurD in the absence and presence of the inhibitor, *N*-({3-[({4-[(*Z*)- (2,4-dioxo-1,3-thiazolidin-5-ylidene)methyl]phenyl}amino)methyl]phenyl}carbonyl)-D-glutamic acid (5). Because the two gadolinium ions were attached to domains 2 and 3, the inter-gadolinium distance distribution reflects the position and orientation of domain 3 with respect to domain 2 (Figure 1c). The distance measurement was performed using four-pulse DEER experiments on a Q-band spectrometer, with a dipolar evolution time as long as 3.9 μs (Figure 3). Unlike $D12_{145–260}$ or $D12_{170–260}$, which have a defined distance between Gd^{3+} ions (Figure 2c and d), DEER traces for $MurD_{260–360}$, especially in the absence of the inhibitor, showed that the oscillation disappears after ~0.4 μs (Figure 3a and c), which implies the existence of multiple Gd^{3+}–Gd^{3+} distances and thus multiple conformational states of $MurD_{260–360}$ in the absence of the inhibitor. The distance distribution for $MurD_{260–360}$ in the absence of the inhibitor indeed showed a broad major peak whose top was located at 3.56 nm (Figure 3e). Although the position of the peak top is close to that expected from the crystal structure of MurD in the open conformation (PDB code: 1e0d.pdb, 3.21 ± 0.20 nm) (8) (Figure S5a), there was a small but significant gap between the two distances. This indicates that the major conformational state in solution is somewhat different from that observed in the crystal structure (8).

To obtain more detailed information about the conformational state of apo MurD in solution, the DEER distance distribution was compared with that obtained using MD simulation (41). Although gadolinium ion and CLaNP-5 tag were not included in the simulation, the positions of the gadolinium ion were estimated by superimposing the coordinates of domains 2 and 3 containing the coordinates of the lanthanide ion so that the inter-gadolinium distances can be estimated for each of the coordinates. The trajectory of the inter-gadolinium distance of the MD simulation showed that each of the conformational states of MurD has a distinct inter-

gadolinium distance (Figure 4), indicating that inter-gadolinium distances obtained by DEER measurement clearly reflected differences among the conformational states of MurD. Importantly, the distances estimated for the coordinates from MD simulations are all within the range of the DEER distance distribution (Figure 4), which highlights the consistency and reliability of the two data sets. The MD trajectory showed that the major conformational state has an inter-gadolinium distance of ~3.6 nm (Figure 4), which coincides with the position of the peak top of the DEER distance distribution for $MurD_{260–360}$ in the absence of the ligand (3.56 nm) (Figure 3e). The major conformational states in MD simulation show that domain 3 tilted from that in the crystal structure in the open conformation by ~20° (Figure 4). Thus, both MD simulation and DEER distance measurement highlighted the major conformational state of apo MurD in solution.

MD simulation also highlighted a variety of conformational states of MurD (Figure 4), which well explains the broad distance distribution obtained from DEER experiments for MurD in the absence of the inhibitor. The broad distance distribution indicates that MurD exists as an ensemble of a variety of conformational states in solution that have not observed in crystal structures. The FWHM for the major peak in the absence of the inhibitor was estimated as 1.28 nm, which is much wider than that observed for $D12_{145–260}$ and $D12_{170–260}$ (0.7-0.8 nm)(Figures 2e, f and 3e). Note that the wide distance distribution for $MurD_{260–360}$ was also supported by the theoretical DEER traces (Figure S6), in which the distance distribution for σ = 1.0 nm indicated the DEER traces very similar to that observed for $MurD_{260–360}$ in the absence of the ligand (Figure 3c). The distance distribution also covers the distance expected from the closed conformation as seen in the crystal structure of MurD in complex with the ligands or the inhibitor (Figure S5b), implying that the conformational ensemble of MurD includes the closed conformation even in the absence of the inhibitor.

On the other hand, the DEER measurement for $MurD_{260–360}$ in the presence of the inhibitor showed a narrower distance distribution (Figure 3f). In the presence of the inhibitor, the distance distribution obtained from Tikhonov regularization showed that the FWHM for the

major peak decreased from 1.28 nm to 1.14 nm, and the peak top shifted from 3.56 nm to 4.10 nm (Figure 3e and f), which corresponds to the distance expected for the crystal structure of MurD in the closed conformation (4.35 ± 0.25 nm) (Figure S5b) (5). Although the distance distribution of $MurD_{260–360}$ became narrower in the presence of the inhibitor, the FWHM of 1.14 nm for $MurD_{260–360}$ in complex with the inhibitor is still wider than that observed for $D12_{145–260}$ or $D12_{170–260}$ (0.7-0.8 nm) (Figures 2 and 3). As the binding is expected to be saturated given the affinity and concentrations of MurD and the inhibitor (10), the wider distance distribution for $MurD_{260–360}$ in complex with the inhibitor suggests residual conformational variety of MurD even in complex with the inhibitor. Note that single Gaussian fitting showed that the overall average distance shifted from 3.78 to 4.21 nm after addition of the inhibitor (Figure S7), supporting the inhibitor-induced conformational change of MurD. Thus, the results showed that MurD in solution exists in an ensemble of a variety of conformational states, and the binding of the inhibitor shifts the population toward the closed conformation.

DISCUSSION

MurD, a protein enzyme consisting of three domains, is known to undergo drastic conformational changes during its catalytic process. Previous crystallographic studies have concluded that in the absence of ligands, MurD exists in an open conformation (8), whereas in the presence of ligands or inhibitors it exists in a closed conformation (1, 2, 5, 9). Although it has been believed that MurD takes a specific conformational state as seen in the crystal structure, the DEER distance measurement carried out for MurD in this study has shown wide distance distribution for the apo state (Figure 3e), indicating that apo MurD exists in a wide variety of conformational states in solution. DEER distance distribution for $MurD_{260–360}$ shows that the FWHM for the major peak in the absence of the inhibitor is 1.28 nm, which is much wider than that obtained for $D12_{145–260}$ and $D12_{170–260}$ (0.7-0.8 nm), in which the two gadolinium ions are fixed on the same domain (Figures 2e, f and 3e). The increased distance distribution of apo $MurD_{260–360}$ indicates the conformational variation of MurD, especially variation in position and/or orientation of domain 3 with respect to domain 2.

The distance distribution for $MurD_{260–360}$ in the absence of the ligand covers not only the distance expected for the open conformation but also that for the closed conformation (Figure 3 and Figure S5), and thus suggests that MurD can also exist in a closed conformation even in the absence of the ligand. The existence of the closed conformation in the absence of the ligands was initially implied by the previous NMR observation: The resonances derived from the interface between the domains 2 and 3 in the closed conformation show significant line broadening in the absence of the ligand (10). The resonance broadening in NMR indicates the exchange among multiple states in the μs–ms time scale. Furthermore, our experimental data from neutron spin echo (NSE) and small-angle X-ray scattering (SAXS) as well as MD simulation (41) also indicated that conformational ensemble and amplitude of domain motion are larger in the apo state than in the ligand-bound state. Collectively, our NMR, EPR, NSE, SAXS, and MD data all suggest that MurD at apo state in solution is much more dynamic than previously thought and exists in multiple conformational states in exchange, including open and closed conformational

states. The details about the conformational variation of apo MurD is further discussed based on all possible experimental and computational data in our other paper (41).

It should be also noted that the DEER distance distribution for $MurD_{260–360}$ in the absence of the ligand showed a major peak with a maximum height of 3.56 nm, which is different from the inter-gadolinium distance expected from the crystal structure of apo MurD (1e0d), but coincides with the distance estimated for the major conformational states of MurD in the MD simulation (~3.6 nm) (Figure 4) (41). The typical MD coordinates of MurD having an inter-gadolinium distance of ~3.6 nm show domain 3 rotated from the crystal open structure by ~20° (Figure 4), which results in a wide, open cavity for ATP binding (Figure S8). Thus, the crystal structure of apo MurD has the orientation of the domain 3 hindered by crystal packing. Given the fact that the cavity for nucleotide binding is more widely exposed in this major open conformation, this conformation can be beneficial for capturing ATP molecules.

In contrast to the wide conformational distribution of apo MurD, the presence of the inhibitor narrows down the population toward the closed conformation (Figure 3f). The peak top of the DEER distance distribution of $MurD_{260-360}$ (4.10 nm) roughly matches to the distance expected from the crystal structure in the closed conformation (4.35 ± 0.25 nm) (5). Thus, the data indicate that MurD in solution exists in a wide variety of conformational states in the absence of the ligand, but the binding of the ligand causes MurD to settle down in a specific conformational state.

In this study, we used DEER distance measurements for a multidomain protein attached with a rigid double-arm gadolinium-chelating tag to characterize the conformational states of the protein in the absence and presence of the inhibitor. Given the fact that the gadolinium ion can be attached to specific positions of a protein by the use of the tag, this strategy can be applied to other proteins as well. Our results also demonstrate that the combination of inter-gadolinium distance measurement by DEER EPR and MD simulation visualizes the conformational ensemble of a multi-domain protein and its conformational change upon binding to the inhibitor. Simple but reliable distance information obtained from DEER distance measurement is

corroborated by MD simulation. The DEER distance measurement is often performed for several different sets of the protein samples having the paramagnetic centers at different sites, in order to obtain detailed structural information of the protein. However, design of the multiple mutations for the introduction of the paramagnetic centers within appropriate distances (< ~8 nm) is not always straightforward. Instead of acquiring multiple sets of the DEER distance distribution, our study has demonstrated the combined use of MD simulation and DEER distance measurement to obtain experimentally guided, detailed structural information for investigation of protein structure as an ensemble.

This strategy will be efficient not only in structural studies, but also in the evaluation of drug candidates in drug design. Conformational states and changes of a protein in the absence and presence of the drug candidates should be a good probe for drug validation. Thus, the information about the conformational states in solution is essential in drug design and evaluation. Furthermore, given the usefulness of the CLaNP-5 tag in protein NMR study, different sets of structural information can, in principle, be added: Attachment of the lanthanide ion that induces anisotropic paramagnetic effects enables the observation of a variety of paramagnetic effects in NMR that contain long-range quantitative structural information. The integrated structural analysis that includes these NMR-derived paramagnetic effects will further expand the ability of the strategy to explore protein structure and dynamics in solution.

SUPPORTING MATERIAL

Supporting Material can be found online at https://doi.org/

AUTHOR CONTRIBUTIONS

T.S. designed the research project. T.S. and S.H. mainly carried out the research. M.A., S.H., T.S., and T.N. performed EPR measurement and analysis. S.H., T.S., and H.K. performed NMR measurement and analysis. S.H. and K.S. conducted preparation of the lanthanide tags and protein samples. T.S., H.N., and K.I. discussed the results and wrote the manuscript. All authors read and approved the final manuscript.

ACKNOWLEDGMENTS

We thank T. Kanaba and H. Hara (Bruker) for fruitful discussions and suggestions during the early phase of the project. This work was partially supported by JSPS KAKENHI (17H05657, 17H05867, 18H05229, and 19K06504 to T.S. and 19H05769 to K.I.), JST PRESTO Program to T.S., JST FOREST Program to T.S., AMED Practical Research Project for Rare/Intractable Diseases (JP21ek0109437) to T.S. This work was also partially supported by Toyota Riken Scholar, Takeda Science Foundation Grant, The Sumitomo Foundation, Astellas Foundation for Research on Metabolic Disorders, Senri Life Science Foundation, The Nakajima Foundation, The Asahi Glass Foundation, Akiyama Life Science Foundation Grants-in-Aid, and Northern Advancement Center for Science and Technology Grants-in-Aid to T.S. The EPR measurements were supported by Nanotechnology Platform Program <Molecule and Material Synthesis> (JPMXP09S18MS0006, JPMXP09S17MS0002, JPMXP09S16MS0040) of the Ministry of Education, Culture, Sports, Science and Technology (MEXT), Japan. The NMR experiments were performed at Hokkaido University Advanced NMR Facility, a member of NMR Platform.

REFERENCES

1. Smith, C.A. 2006. Structure, Function and Dynamics in the mur Family of Bacterial Cell Wall Ligases. Journal of Molecular Biology. 362: 640–655.

2. Bertrand, J.A., G. Auger, L. Martin, E. Fanchon, D. Blanot, D. Le Beller, J. van Heijenoort, and O. Dideberg. 1999. Determination of the MurD mechanism through crystallographic analysis of enzyme complexes. Journal of Molecular Biology. 289: 579–590.

3. Pratviel-Sosa, F., F. Acher, F.O. Trigalo, D. Blanot, R. Azerad, and J. Heijenoort. 1994. Effect of various analogues of D-glutamic acid on the D-glutamate-adding enzyme from Escherichis coli. FEMS Microbiology Letters. 115: 223–228.

4. Bouhss, A., S. Dementin, C. Parquet, D. Mengin-Lecreulx, J.A. Bertrand, D. Le Beller, O. Dideberg, J. van Heijenoort, and D. Blanot. 1999. Role of the Ortholog and Paralog Amino Acid Invariants in the Active Site of the UDP-MurNAc- l-alanine: d-glutamate Ligase (MurD). Biochemistry. 38: 12240–12247.

5. Zidar, N., T. Tomašić, R. Šink, V. Rupnik, A. Kovač, S. Turk, D. Patin, D. Blanot, C. Contreras-Martel, A. Dessen, M. Müller Premru, A. Zega, S. Gobec, L. Peterlin Mašič, and D. Kikelj. 2010. Discovery of Novel 5-Benzylidenerhodanine and 5-Benzylidenethiazolidine-2,4-dione Inhibitors of MurD Ligase. J. Med. Chem. 53: 6584–6594.

6. Tomašić, T., R. Šink, N. Zidar, A. Fic, C. Contreras-Martel, A. Dessen, D. Patin, D. Blanot, M. Müller Premru, S. Gobec, A. Zega, D. Kikelj, and L.P. Mašič. 2012. Dual Inhibitor of MurD and MurE Ligases from Escherichia coli and Staphylococcus aureus. ACS Med. Chem. Lett. 3: 626–630.

7. Perdih, A., M. Hrast, H. Barreteau, S. Gobec, G. Wolber, and T. Solmajer. 2014. Inhibitor Design Strategy Based on an Enzyme Structural Flexibility: A Case of Bacterial MurD Ligase. J. Chem. Inf. Model. 54: 1451–1466.

8. Bertrand, J.A., E. Fanchon, L. Martin, L. Chantalat, G. Auger, D. Blanot, J. van Heijenoort, and O. Dideberg. 2000. “Open” structures of MurD: domain movements and structural similarities with folylpolyglutamate synthetase. Journal of Molecular Biology. 301: 1257–1266.

9. Kotnik, M., J. Humljan, C. Contreras-Martel, M. Oblak, K. Kristan, M. Hervé, D. Blanot, U. Urleb, S. Gobec, A. Dessen, and T. Solmajer. 2007. Structural and Functional Characterization of Enantiomeric Glutamic Acid Derivatives as Potential Transition State Analogue Inhibitors of MurD Ligase. Journal of Molecular Biology. 370: 107–115.

10. Saio, T., K. Ogura, H. Kumeta, Y. Kobashigawa, K. Shimizu, M. Yokochi, K. Kodama, H. Yamaguchi, H. Tsujishita, and F. Inagaki. 2015. Ligand-driven conformational changes of MurD visualized by paramagnetic NMR. Sci. Rep. 5: 16685.

11. Perdih, A., M. Kotnik, M. Hodoscek, and T. Solmajer. 2007. Targeted molecular dynamics simulation studies of binding and conformational changes in E. coli MurD. Proteins: Structure, Function, and Bioinformatics. 68: 243–254.

12. Perdih, A., and T. Solmajer. 2012. MurD ligase from Escherichia coli: C-terminal domain closing motion. Computational and Theoretical Chemistry. 979: 73–81.

13. Puljung, M.C., H.A. DeBerg, W.N. Zagotta, and S. Stoll. 2014. Double electron-electron resonance reveals cAMP-induced conformational change in HCN channels. Proc. Natl. Acad. Sci. U.S.A. 111: 9816–9821.

14. Abdelkader, E.H., A. Feintuch, X. Yao, L.A. Adams, L. Aurelio, B. Graham, D. Goldfarb, and G. Otting. 2015. Protein conformation by EPR spectroscopy using gadolinium tags clicked to genetically encoded p-azido-L-phenylalanine. Chem. Commun. 51: 15898–15901.

15. Manglik, A., T.H. Kim, M. Masureel, C. Altenbach, Z. Yang, D. Hilger, M.T. Lerch, T.S. Kobilka, F.S. Thian, W.L. Hubbell, R.S. Prosser, and B.K. Kobilka. 2015. Structural Insights into the Dynamic Process of β2-Adrenergic Receptor Signaling. Cell. 161: 1101–1111.

16. Martorana, A., G. Bellapadrona, A. Feintuch, E. Di Gregorio, S. Aime, and D. Goldfarb. 2014. Probing Protein Conformation in Cells by EPR Distance Measurements using Gd^{3+} Spin Labeling. J. Am. Chem. Soc. 136: 13458–13465.

17. Saio, T., and K. Ishimori. 2019. Accelerating structural life science by paramagnetic lanthanide probe methods. Biochimica et Biophysica Acta (BBA) - General Subjects.

18. Nitsche, C., and G. Otting. 2017. Pseudocontact shifts in biomolecular NMR using paramagnetic metal tags. Progress in Nuclear Magnetic Resonance Spectroscopy. 98-99: 20–49.

19. Fielding, A., M. Concilio, G. Heaven, and M. Hollas. 2014. New Developments in Spin Labels for Pulsed Dipolar EPR. Molecules 2014, Vol. 19, Pages 16998-17025. 19: 16998–17025.

20. Cunningham, T.F., M.R. Putterman, A. Desai, W.S. Horne, and S. Saxena. 2015. The Double-Histidine Cu^{2+}-Binding Motif: A Highly Rigid, Site-Specific Spin Probe for Electron Spin Resonance Distance Measurements. Angewandte Chemie. 127: 6428–6432.

21. Keizers, P.H.J., J.F. Desreux, M. Overhand, and M. Ubbink. 2007. Increased Paramagnetic Effect of a Lanthanide Protein Probe by Two-Point Attachment. J. Am. Chem. Soc. 129: 9292–9293.

22. Saio, T., K. Ogura, M. Yokochi, Y. Kobashigawa, and F. Inagaki. 2009. Two-point anchoring of a lanthanide-binding peptide to a target protein enhances the paramagnetic anisotropic effect. J Biomol NMR. 44: 157–166.

23. Barthelmes, K., A.M. Reynolds, E. Peisach, H.R.A. Jonker, N.J. DeNunzio, K.N. Allen, B. Imperiali, and H. Schwalbe. 2010. Engineering Encodable Lanthanide-Binding Tags into Loop Regions of Proteins. J. Am. Chem. Soc. 133: 808–819.

24. Welegedara, A.P., Y. Yang, M.D. Lee, J.D. Swarbrick, T. Huber, B. Graham, D. Goldfarb, and G. Otting. 2017. Double-Arm Lanthanide Tags Deliver Narrow Gd^{3+}–Gd^{3+} Distance Distributions in Double Electron–Electron Resonance (DEER) Measurements. Chemistry - A European Journal. 23: 11694–11702.

25. Keizers, P.H.J., A. Saragliadis, Y. Hiruma, M. Overhand, and M. Ubbink. 2008. Design, Synthesis, and Evaluation of a Lanthanide Chelating Protein Probe: CLaNP-5 Yields Predictable Paramagnetic Effects Independent of Environment. J. Am. Chem. Soc. 130: 14802–14812.

26. Lescanne, M., S.P. Skinner, A. Blok, M. Timmer, L. Cerofolini, M. Fragai, C. Luchinat, and M. Ubbink. 2017. Methyl group assignment using pseudocontact shifts with PARAssign. J Biomol NMR. 69: 183–195.

27. Guan, J.-Y., P.H.J. Keizers, W.-M. Liu, F. Löhr, S.P. Skinner, E.A. Heeneman, H. Schwalbe, M. Ubbink, and G. Siegal. 2013. Small-Molecule Binding Sites on Proteins Established by Paramagnetic NMR Spectroscopy. J. Am. Chem. Soc. 135: 5859–5868.

28. Keizers, P.H.J., B. Mersinli, W. Reinle, J. Donauer, Y. Hiruma, F. Hannemann, M. Overhand, R. Bernhardt, and M. Ubbink. 2010. A Solution Model of the Complex Formed by Adrenodoxin and Adrenodoxin Reductase Determined by Paramagnetic NMR Spectroscopy. Biochemistry. 49: 6846–6855.

29. Šink, R., M. Kotnik, A. Zega, H. Barreteau, S. Gobec, D. Blanot, A. Dessen, and C. Contreras-Martel. 2016. Crystallographic Study of Peptidoglycan Biosynthesis Enzyme MurD: Domain Movement Revisited. PLoS ONE. 11: e0152075.

30. Kobashigawa, Y., H. Kumeta, K. Ogura, and F. Inagaki. 2009. Attachment of an NMR-invisible solubility enhancement tag using a sortase-mediated protein ligation method. J Biomol NMR. 43: 145–150.

31. Saio, T., and F. Inagaki. 2016. NMR Structural Biology Using Paramagnetic Lanthanide Probe. In: Advanced Methods in Structural Biology. Tokyo: Springer Japan. pp. 315–340.

32. Saio, T., and F. Inagaki. 2018. Structural Study of Proteins by Paramagnetic Lanthanide Probe Methods. In: Experimental Approaches of NMR Spectroscopy. Singapore: Springer, Singapore. pp. 227–252.

33. Delaglio, F., S. Grzesiek, G.W. Vuister, G. Zhu, J. Pfeifer, and A. Bax. 1995. NMRPipe: a multidimensional spectral processing system based on UNIX pipes. J Biomol NMR. 6: 277–293.

34. Schmitz, C., M.J. Stanton-Cook, X.-C. Su, G. Otting, and T. Huber. 2008. Numbat: an interactive software tool for fitting $\Delta\chi$-tensors to molecular coordinates using pseudocontact shifts. J Biomol NMR. 41: 179–189.

35. Schwieters, C.D., J.J. Kuszewski, and M. Clore. 2006. Using Xplor–NIH for NMR molecular structure determination. Progress in Nuclear Magnetic Resonance Spectroscopy. 48: 47–62.

36. Saio, T., K. Ogura, K. Shimizu, M. Yokochi, T.R. Burke Jr, and F. Inagaki. 2011. An NMR strategy for fragment-based ligand screening utilizing a paramagnetic lanthanide probe. J Biomol NMR. 51: 395–408.

37. Schüttelkopf, A.W., and D.M.F. van Aalten. 2004. PRODRG: a tool for high-throughput crystallography of protein–ligand complexes. Acta Crystallogr D Biol Crystallogr. 60: 1355–1363.

38. Pedretti, A., L. Villa, and G. Vistoli. 2002. VEGA: a versatile program to convert, handle and visualize molecular structure on Windows-based PCs. Journal of Molecular Graphics and Modelling. 21: 47–49.

39. Jeschke, G., V. Chechik, P. Ionita, A. Godt, H. Zimmermann, J. Banham, C.R. Timmel, D. Hilger, and H. Jung. 2006. DeerAnalysis2006—a comprehensive software package for analyzing pulsed ELDOR data. Appl. Magn. Reson. 30: 473–498.

40. Dalaloyan, A., M. Qi, S. Ruthstein, S. Vega, A. Godt, A. Feintuch, and D. Goldfarb. 2015. Gd(III)–Gd(III) EPR distance measurements – the range of accessible distances and the impact of zero field splitting. Phys. Chem. Chem. Phys. 17: 18464–18476.

41. Nakagawa, H., Saio, T., Nagao, M., Inoue, R., Sugiyama, M., Ajito, S., Tominaga, T., Kawakita, Y. Conformational dynamics of a multi-domain protein explored by neutron scattering and computational analysis. *submitted*.

Table 1 Magnetic susceptibility tensors of Yb^{3+} attached to $D12_{145}$, $D12_{170}$, and $D12_{260}$.

Position	Lanthanide ion	$\Delta\chi_{ax}$ [a]	$\Delta\chi_{rh}$ [a]	α [b]	β [b]	γ [b]	x [c]	y [c]	z [c]
M145C/D148C	Yb^{3+}	7.3 ± 0.3	1.6 ± 0.5	80	70	172	46.9 ± 0.3	9.8 ± 0.3	36.1 ± 1.3
	Tm^{3+}	43.7 ± 1.3	11.4 ± 2.0	80	71	171			
Q170C/V172C	Yb^{3+}	5.7 ± 0.1	1.9 ± 0.1	24	42	151	51.8 ± 0.2	-13.2 ± 0.3	41.7 ± 0.3
E260C/K262C[d]	Yb^{3+}	8.4 ± 0.5	0.6 ± 0.7	137	69	22	14.3 ± 0.5	-4.7 ± 0.5	38.4 ± 1.3
	Tm^{3+}	47.0 ± 2.3	8.5 ± 5.2	137	72	59			

[a]$\Delta\chi_{ax}$ and $\Delta\chi_{rh}$ values are in 10^{-32} (m^3), and error estimates were obtained by Monte Carlo protocol using 100 partial pseudo-contact shift (PCS) data sets, in which 30% of the input data were randomly deleted. [b]Euler angles (α, β, γ) are represented in ZYZ convention in degrees. [c]Position of the lanthanide ion is expressed in angstrom (Å) as a coordinate in the crystal structure of MurD (PDB ID: 3uag). [d] Parameters determined in a previous study (10).

`

Figure legends

Figure 1 Gadolinium tagging of MurD. The positions of metals in MurD domain 1–2 M145C/D148C/C151A/E260C/K262C ($D12_{145–260}$) (a), MurD domain 1–2 Q170C/V172C/E260C/K262C ($D12_{170–260}$) (b), and MurD E260C/K262C/N360C/D362C ($MurD_{260–360}$) (c) are shown as red spheres in the crystal structure of MurD [Protein Data Bank (PDB) ID: 3uag]. Domains 1, 2, and 3 are presented in green, blue, and pink, respectively. The distance between lanthanoid ions are indicated by a red arrow. (d) The chemical structure of Caged Lanthanide NMR Probe 5 (CLaNP-5) tag. (e) Close-up views of the positions of lanthanoid ions fixed on MurD. The residues that were mutated to cysteine residue for ligation with the CLaNP-5 tag are shown as red stick model. The distances between C_β atoms are indicated.

Figure 2 Four-pulse DEER distance measurement for $D12_{145–260}$ and $D12_{170–260}$. The experiment was performed on ~30 μL of 200 μM frozen solution of $D12_{145–260}$ (a, c, and e) or $D12_{170–260}$ (b, d, and f) in 70% D_2O/30% glycerol-d_8 at 10 K. (a and b) Normalized DEER traces fitted with appropriate background decay (in red). (c and d) Same DEER trace after background removal along with the fits obtained either by Tikhonov regularization (orange) or fitting to single Gaussian (blue). (e and f) Distance distribution obtained by the two different fits shown in panels c and d. The data were analyzed using the program DeerAnalysis 2016. DEER, double electron–electron resonance.

Figure 3 Four-pulse DEER distance measurement for $MurD_{260–360}$. The experiment was performed on ~30 μL of 150 μM frozen solution of $MurD_{260–360}$ in the absence (a, c, and e) and presence (b, d, and f) of the inhibitor in 70% D_2O/30% glycerol-d_8 at 10 K. (a and b) Normalized DEER traces fitted with appropriate background decay (in red). (c and d) DEER traces after background removal along with the fits obtained using Tikhonov regularization. (e and f) Distance distributions obtained by the fit shown in panels c and d. The shaded region shows an estimate of the range of distance distributions that arise from varying background subtraction. The arrows indicate the distance between the gadolinium ions expected from the crystal structures of MurD in open (PDB code 1e0d, 3.21 nm) and closed (PDB code 3uag, 4.35 nm) conformations. The data were analyzed using the program DeerAnalysis 2016. DEER, double electron–electron

resonance.

Figure 4 Comparison between DEER distance measurement and molecular dynamics (MD) simulation for apo MurD. The representative coordinates observed in MD simulations are shown with corresponding positions in the trajectories of the inter-gadolinium distance. The coordinates from MD calculation are colored blue and superimposed on domain 2 of the crystal structure of MurD in the open conformation (PDB code: 1e0d), in which domains 1, 2, and 3 are presented in green, blue, and pink, respectively. The changes in rotation and translation of domain 3 are indicated. The DEER distance distributions for $MurD_{260–360}$ in the absence of the inhibitor are shown on the right, in which horizontal and vertical axes represent relative population and inter-gadolinium distance, respectively. The shaded region in orange shows an estimate of the range of distance distributions that arise from varying background subtraction. DEER, double electron–electron resonance.

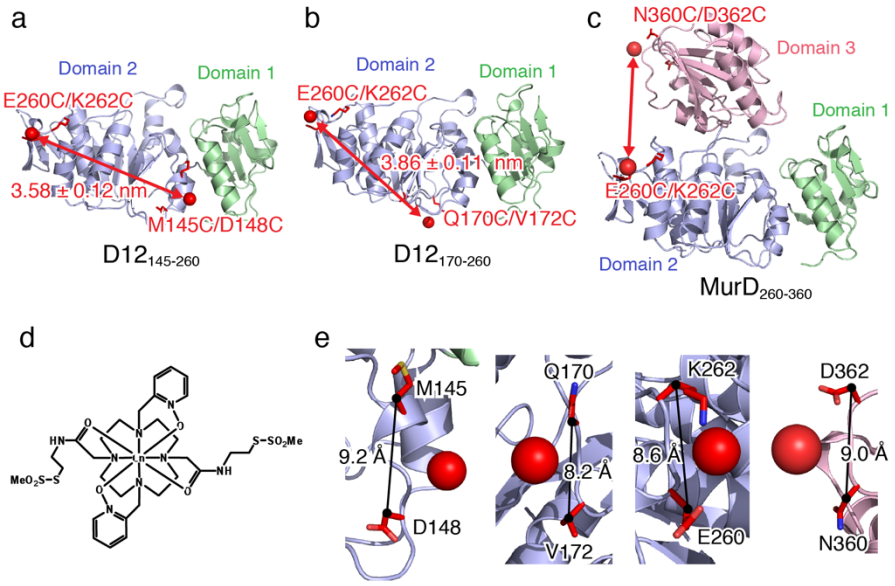

Figure 1 Gadolinium tagging of MurD. The positions of metals in MurD domain 1–2 M145C/D148C/C151A/E260C/K262C ($D12_{145–260}$) (a), MurD domain 1–2 Q170C/V172C/E260C/K262C ($D12_{170–260}$) (b), and MurD E260C/K262C/N360C/D362C ($MurD_{260–360}$) (c) are shown as red spheres in the crystal structure of MurD [Protein Data Bank (PDB) ID: 3uag]. Domains 1, 2, and 3 are presented in green, blue, and pink, respectively. The distance between lanthanoid ions are indicated by a red arrow. (d) The chemical structure of Caged Lanthanide NMR Probe 5 (CLaNP-5) tag. (e) Close-up views of the positions of lanthanoid ions fixed on MurD. The residues that were mutated to cysteine residue for ligation with the CLaNP-5 tag are shown as red stick model. The distances between C_β atoms are indicated.

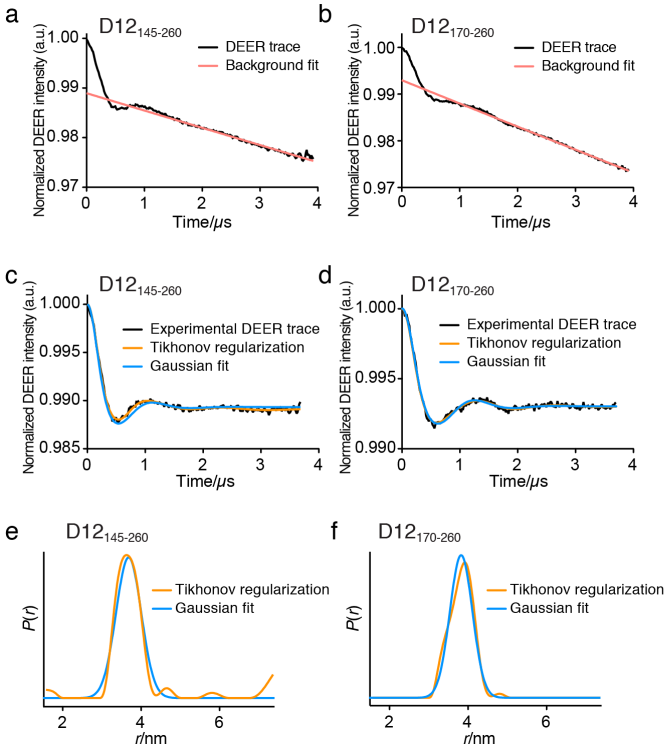

Figure 2 Four-pulse DEER distance measurement for D12$_{145–260}$ and D12$_{170–260}$. The experiment was performed on ~30 μL of 200 μM frozen solution of D12$_{145–260}$ (a, c, and e) or D12$_{170–260}$ (b, d, and f) in 70% D_2O/30% glycerol-d_8 at 10 K. (a and b) Normalized DEER traces fitted with appropriate background decay (in red). (c and d) Same DEER trace after background removal along with the fits obtained either by Tikhonov regularization (orange) or fitting to single Gaussian (blue). (e and f) Distance distribution obtained by the two different fits shown in panels c and d. The data were analyzed using the program DeerAnalysis 2016. DEER, double electron–electron resonance.

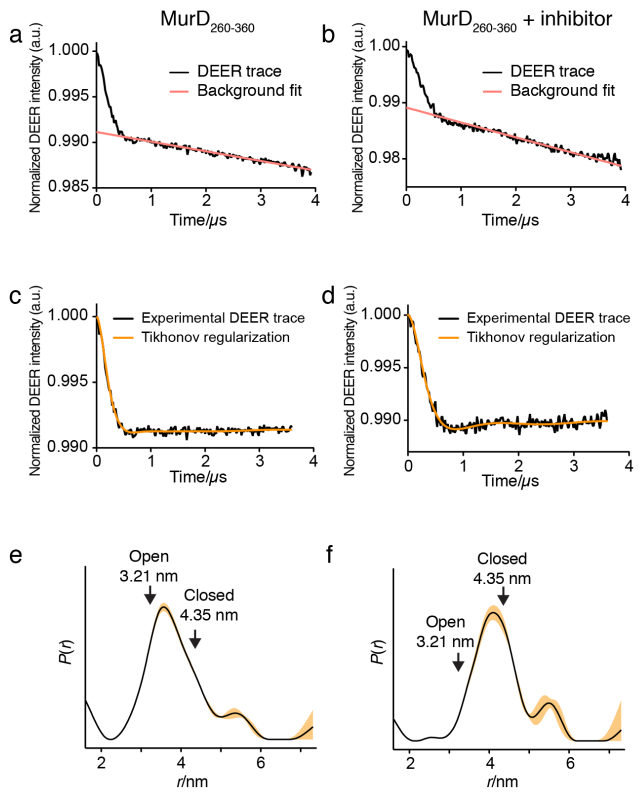

Figure 3 Four-pulse DEER distance measurement for MurD$_{260\text{-}360}$. The experiment was performed on ~30 µL of 150 µM frozen solution of MurD$_{260–360}$ in the absence (a, c, and e) and presence (b, d, and f) of the inhibitor in 70% D_2O/30% glycerol-d_8 at 10 K. (a and b) Normalized DEER traces fitted with appropriate background decay (in red). (c and d) DEER traces after background removal along with the fits obtained using Tikhonov regularization. (e and f) Distance distributions obtained by the fit shown in panels c and d. The shaded region shows an estimate of the range of distance distributions that arise from varying background subtraction. The arrows indicate the distance between the gadolinium ions expected from the crystal structures of MurD in open (PDB code 1e0d, 3.21 nm) and closed (PDB code 3uag, 4.35 nm) conformations. The data were analyzed using the program DeerAnalysis 2016. DEER, double electron–electron resonance.

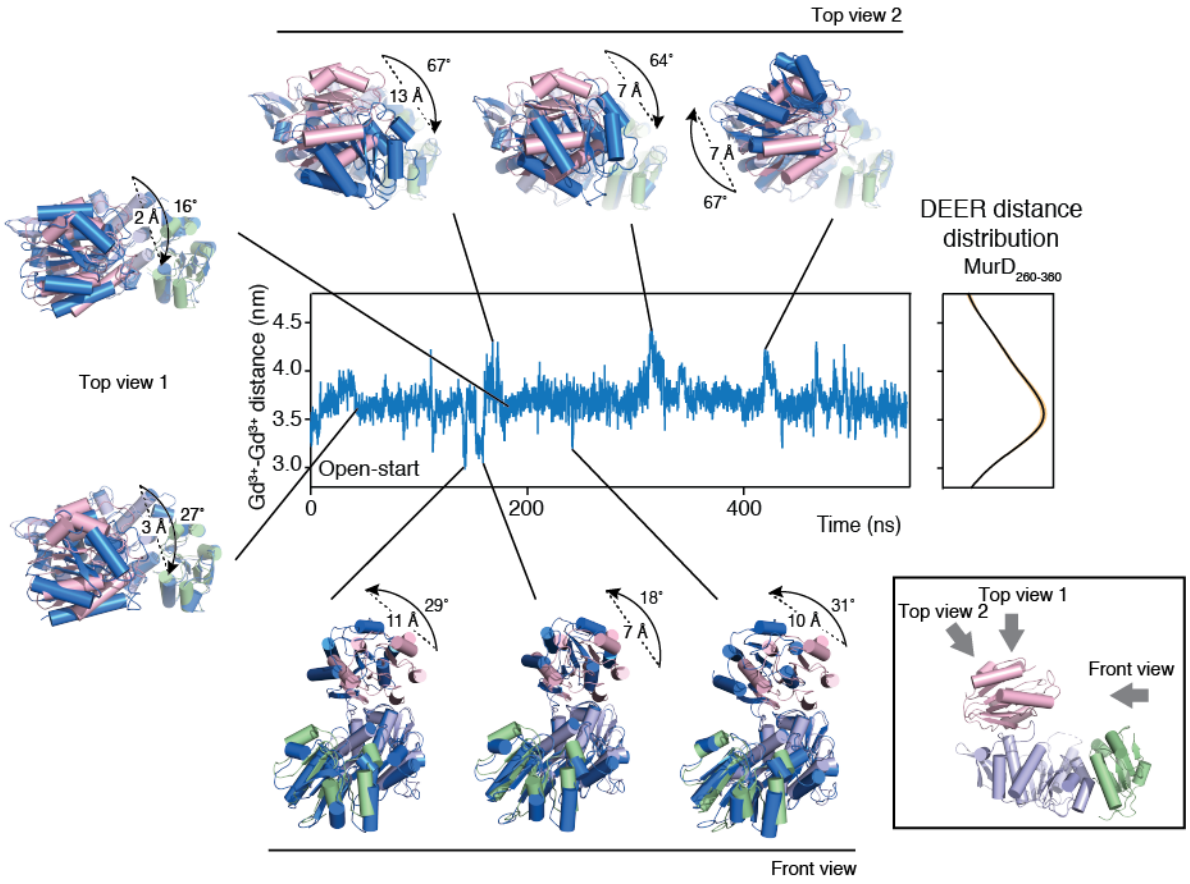

Figure 4 Comparison between DEER distance measurement and molecular dynamics (MD) simulation for apo MurD. The representative coordinates observed in MD simulations are shown with corresponding positions in the trajectories of the inter-gadolinium distance. The coordinates from MD calculation are colored blue and superimposed on domain 2 of the crystal structure of MurD in the open conformation (PDB code: 1e0d), in which domains 1, 2, and 3 are presented in green, blue, and pink, respectively. The changes in rotation and translation of domain 3 are indicated. The DEER distance distributions for $MurD_{260–360}$ in the absence of the inhibitor are shown on the right, in which horizontal and vertical axes represent relative population and inter-gadolinium distance, respectively. The shaded region in orange shows an estimate of the range of distance distributions that arise from varying background subtraction. DEER, double electron–electron resonance.

Supporting information for

Conformational ensemble of a multidomain protein explored by Gd^{3+} electron paramagnetic resonance

T. Saio, S. Hiramatsu, M. Asada, H. Nakagawa, K. Shimizu, H. Kumeta, T. Nakamura, K. Ishimori

Table S1 PCS values observed for $D12_{145}$ attached with CLaNP-5 containing Yb^{3+} and Tm^{3+}.

	Yb^{3+}		Tm^{3+}	
	H^N	N	H^N	N
VAL8	-0.153	-0.148		
ILE10	-0.092	-0.092		
ILE11	-0.007	-0.063	-0.005	-0.060
LEU13	0.000	-0.097	-0.005	-0.104
VAL29	-0.460	-0.552		
VAL33	-0.113	-0.174		
LEU46	-0.207	-0.259		
VAL50	-0.189	-0.208		
LEU57	-0.009	-0.009	-0.123	-0.346
LEU62	-0.033	-0.034		
MET63	-0.033	-0.035	-0.167	-0.264
LEU67	-0.078	-0.027	-0.356	-0.289
ILE68	-0.032	-0.017		
VAL69	-0.008	-0.014		
ILE74	0.086	0.082	0.460	0.337
LEU76	0.055	0.021		
LEU81	-0.006	0.069		
ILE89	-0.014	-0.010	-0.019	-0.018
ILE91	0.010	0.006	0.142	0.142
VAL92	0.025	0.027		
ILE95	0.389	0.431		
LEU97	0.223	0.181	1.466	1.420
ILE106	0.345	0.399	2.132	2.400
VAL107	0.505	0.450		
ILE109	0.368	0.304		
VAL118	0.183	0.188		
LEU121	0.189	0.197		
VAL122	0.227	0.177		
MET125	0.145	0.104	0.952	0.773
VAL131	0.046	0.019		
ILE139	0.467	0.652	2.625	2.710
LEU144	1.631	2.073		
LEU153	0.615	0.535		
LEU156	0.600	0.685		
LEU158	0.352	0.318		
LEU163	0.215	0.212	1.263	1.317
LEU169	0.189	0.170	1.212	1.252
VAL172	0.261	0.225		
ILE176	0.139	0.159	0.853	0.946
LEU177	0.137	0.060	0.930	0.899
VAL179	0.081	0.074		
MET184	0.036	0.055	0.308	0.243
LEU191	0.043	0.061	0.269	0.372
LEU199	0.106	0.069	0.697	0.649
ILE201	0.153	0.172	0.968	0.893
VAL207	0.141	0.129		
VAL209	0.138	0.121		
VAL210	0.100	0.077		
LEU216	0.064	0.028	0.377	0.293
MET218	0.073	0.090	0.446	0.424
ILE220	0.069	0.099	0.423	0.528
VAL228	0.093	0.028		
VAL232	0.050	0.042		
MET234	0.041	0.048	0.257	0.255
LEU248	0.016	0.007	0.188	0.157
VAL250	0.037	0.007		
VAL255	0.032	-0.013		
LEU256	0.024	0.046	0.178	0.246
VAL258	0.021	0.019		
MET261	0.009	0.028	0.108	0.217
LEU263	0.017	0.005	0.165	0.127
LEU273	0.077	0.075	0.472	0.425
LEU276	0.106	0.119	0.646	0.668
LEU278	0.143	0.116	0.853	0.780
LEU284	0.131	0.091	0.719	0.667
LEU290	0.044	0.050	0.272	0.254
LEU293	0.040	0.059	0.292	0.238
LEU299	0.018	0.016	0.222	0.238

Table S2 PCS values observed for $D12_{170}$ attached with CLaNP-5 containing Yb^{3+}.

	H^N	N		H^N	N
GLY5	-0.079	-0.078	VAL122	0.193	0.217
ASN7	-0.051	-0.054	GLY123	0.118	0.394
VAL8	-0.037	-0.046	MET125	0.075	0.104
LEU13	0.012	0.011	VAL131	-0.103	-0.126
LEU18	-0.003	0.023	ILE139	0.150	0.154
LEU25	-0.087	-0.115	LEU141	0.034	0.080
ARG27	-0.128	-0.071	LEU144	0.002	-0.034
GLY28	-0.098	-0.076	LEU158	0.417	0.398
VAL29	-0.088	-0.064	LEU163	0.322	0.345
VAL33	-0.004	0.000	THR165	0.224	0.214
MET34	0.000	-0.039	ILE176	0.364	0.447
GLY42	-0.004	-0.012	LEU177	0.277	0.138
LEU43	0.002	0.006	ASN178	0.206	0.243
LYS45	-0.001	-0.026	VAL179	0.149	0.190
ALA49	-0.005	-0.002	GLY190	0.072	0.089
GLU51	-0.011	-0.006	LEU191	0.065	0.158
HIS53	-0.008	-0.022	GLN192	0.081	0.146
GLY55	0.002	-0.022	LEU199	0.117	0.156
SER56	0.001	0.028	MET218	0.143	0.146
LEU57	0.003	-0.020	ILE220	0.301	0.261
TRP61	-0.006	0.096	GLY231	0.057	0.063
LEU62	0.006	0.011	VAL232	0.046	0.002
MET63	-0.003	-0.001	MET234	0.052	0.110
ALA64	-0.005	-0.019	ASN240	0.007	0.011
ASP66	-0.022	-0.027	LEU248	0.008	0.004
LEU67	-0.026	-0.039	VAL250	0.003	0.070
VAL69	0.004	0.037	GLY252	0.007	-0.074
ALA70	0.008	0.017	VAL255	-0.008	-0.012
LEU76	0.072	-0.002	LEU256	0.008	0.063
HIS78	0.044	0.129	VAL258	0.012	-0.002
ILE89	-0.001	0.004	MET261	0.010	0.027
GLU90	-0.029	0.014	LEU263	0.031	0.034
ILE91	0.014	-0.001	THR270	0.072	0.042
VAL92	0.017	0.014	LEU273	0.083	0.144
GLY93	0.128	0.175	LEU276	0.125	0.184
ILE95	0.153	0.121	LEU278	0.204	0.553
LEU97	-0.041	-0.092	GLY283	-0.076	-0.101
PHE98	-0.006	-0.051	ARG286	-0.070	-0.010
ILE109	0.644	0.659	LEU290	-0.011	-0.006
ASN113	0.155	0.143	LEU293	0.019	0.053
VAL118	0.177	0.193	GLY298	0.044	0.041
LEU121	0.146	0.096	LEU299	0.052	0.063

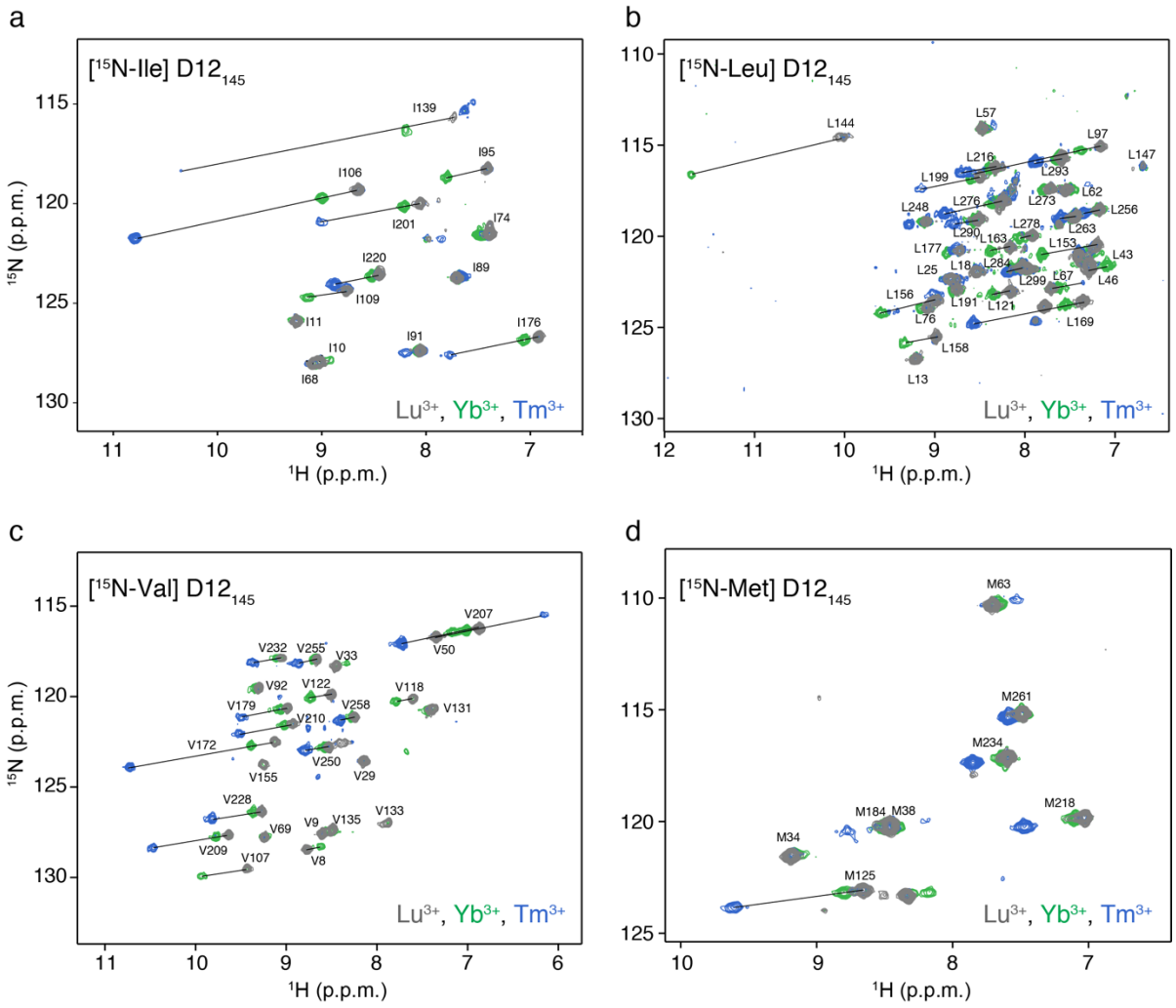

Figure S1 Observation of pseudo-contact shift for D12$_{145}$. Overlay of the ^{1}H–^{15}N heteronuclear single quantum coherence (HSQC) spectra for [^{15}N-Ile] D12$_{145}$ (a), [^{15}N-Leu] D12$_{145}$ (b), [^{15}N-Val] D12$_{145}$ (c), and [^{15}N-Met] D12$_{145}$ (d). The spectra for D12$_{145}$ attached with Lu^{3+}, Yb^{3+}, and Tm^{3+} are colored gray, green, and blue, respectively.

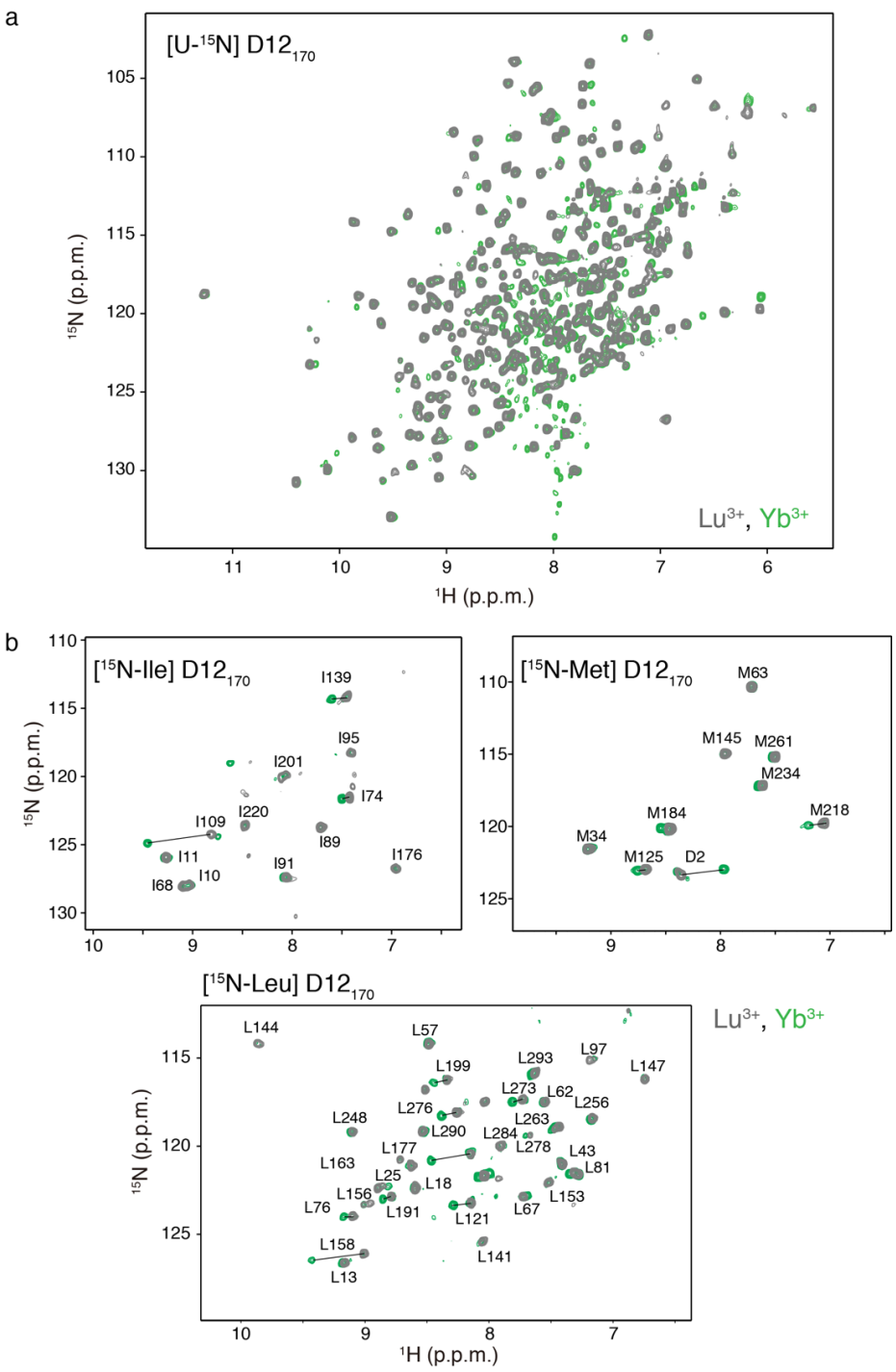

Figure S2 Observation of pseudo-contact shift for D12$_{170}$. Overlay of the ^{1}H-^{15}N heteronuclear single quantum coherence (HSQC) spectra for [U-^{15}N] D12$_{170}$ (a) and amino acid type-selectively ^{15}N labeled D12$_{170}$ (b). The spectra for D12$_{170}$ attached with diamagnetic lanthanoid ion Lu^{3+} and paramagnetic lanthanoid ion Yb^{3+} are colored gray and green, respectively.

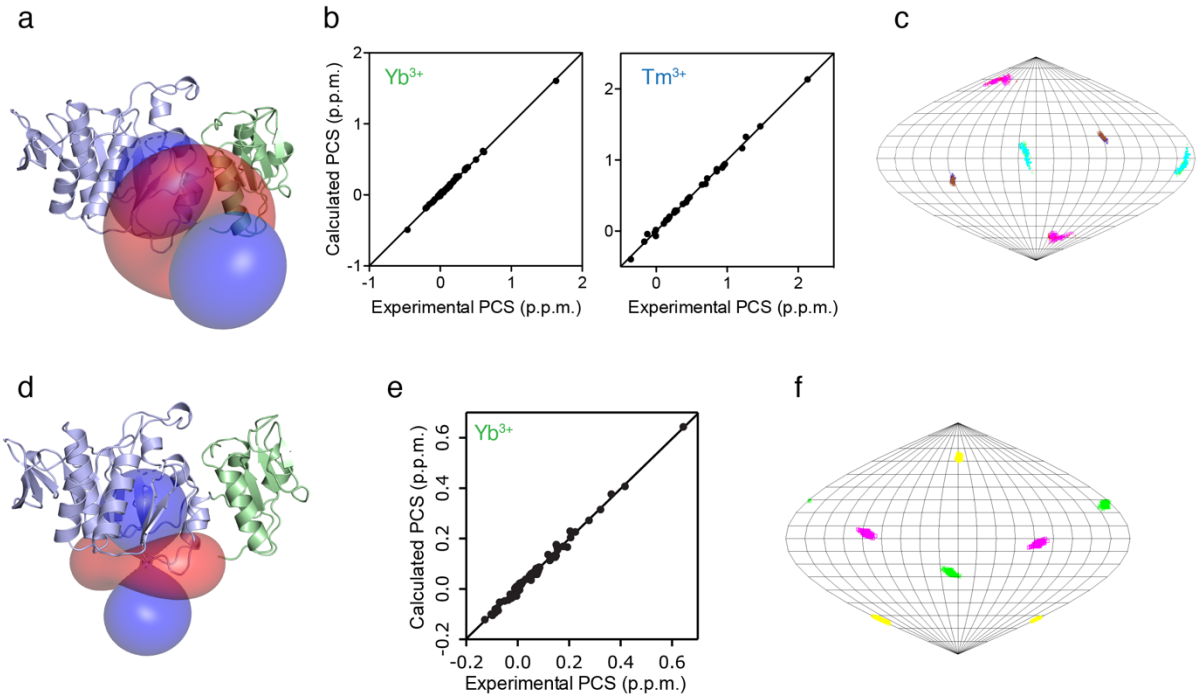

Figure S3 $\Delta\chi$ tensor analysis for $D12_{145}$ and $D12_{170}$. View of the experimentally determined PCS isosurface for $D12_{145}$ (a) and $D12_{170}$ (d) depicting the surface corresponding to ±0.7 ppm induced by Yb^{3+}. Positive and negative PCS values are indicated by blue and red, respectively. Comparison of experimental and back-calculated PCSs of backbone amide protons observed for $D12_{145}$ containing Yb^{3+}/Tm^{3+}-CLaNP-5 (b) and $D12_{170}$ containing Yb^{3+}-CLaNP-5 (e). Orientation of the principal axes of the $\Delta\chi$ tensors of Yb^{3+} and Tm^{3+} in complex with CLaNP-5 fixed on $D12_{145}$ (c) and that of Yb^{3+} in complex with CLaNP-5 fixed on $D12_{170}$ (f), visualized in Sanson–Flamsteed projection. The plots show the points where the principal axes of the $\Delta\chi$ tensor penetrate the sphere. One hundred sets of plots represent the results of the Monte Carlo analysis using the 100 partial PCS data sets in which 30% of the input data were randomly deleted. CLaNP-5, Caged Lanthanide NMR Probe 5; PCS, pseudo-contact shift.

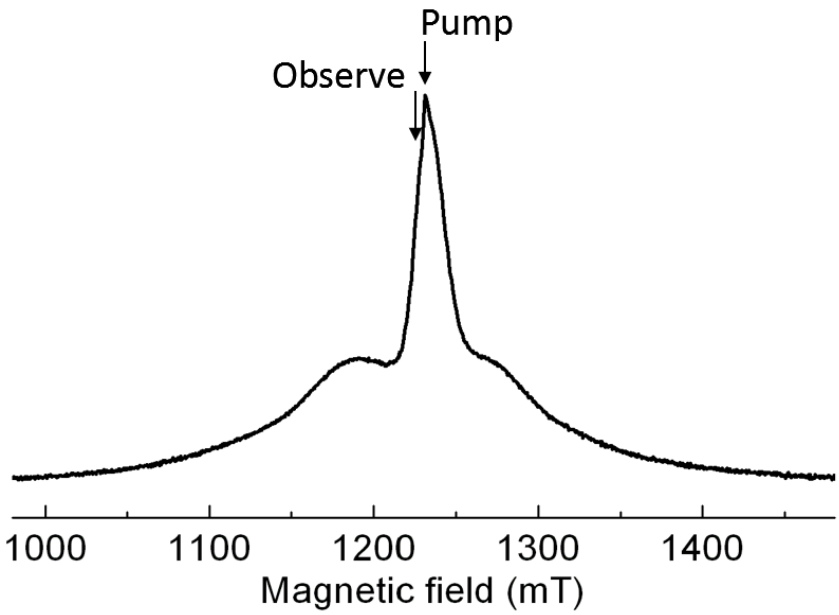

Figure S4 Echo-detected (ED) EPR spectrum around the central |1⁄2> <–> |–1⁄2> transition of D12$_{145–260}$ recorded at 10 K. The measurements were carried out using a two-pulse {π/2–τ–π–τ–echo} sequence with t(π/2) = 16 ns, t(π) = 32 ns, and τ = 200 ns. Positions of the pump and observed frequencies for the DEER experiment are indicated. The ED-EPR spectrum of MurD$_{170–260}$ and MurD$_{260–360}$ look very similar. DEER, double electron–electron resonance; EPR, electron paramagnetic resonance.

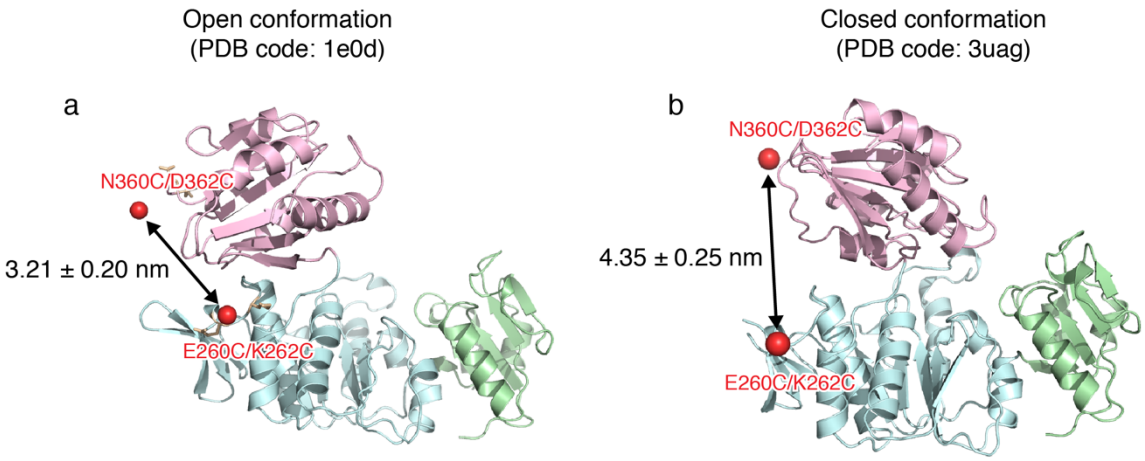

Figure S5 Inter-gadolinium distances of $MurD_{260-360}$ expected from the crystal structures. Crystal structures of MurD in the open (a) and closed (b) conformations with expected inter-gadolinium distances for $MurD_{260–360}$ are indicated. The metal positions for each site were determined using $\Delta\chi$ tensor analysis based on pseudo-contact shifts (PCSs) ($D12_{260}$) or Xplor-NIH docking ($D3_{360}$).

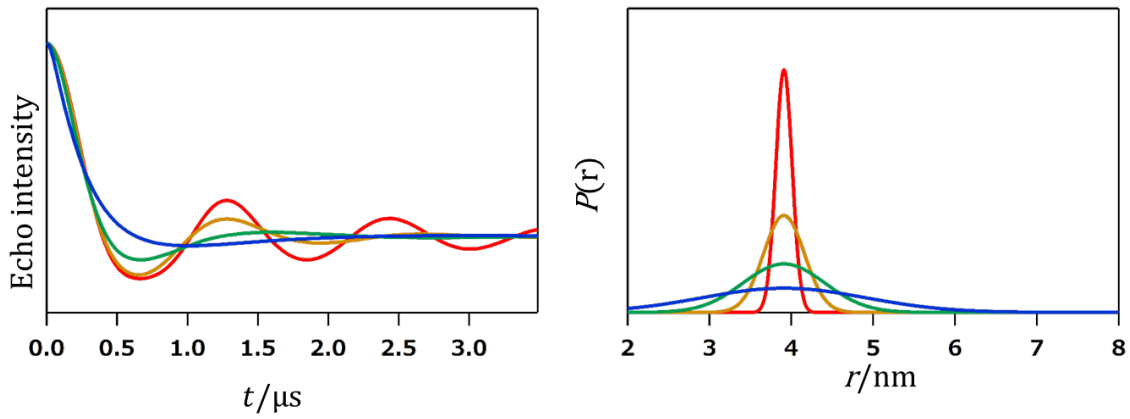

Figure S6 Theoretical DEER traces for the two paramagnetic centers with varying distributions centered at 3.9 nm. Superimposition of theoretical DEER traces (left panel) and distance distributions (right panel), with varying standard deviations of the Gaussian distribution: σ = 0.1 (red), 0.25 (orange), 0.5 (green), 1 (blue) nm. DEER, double electron–electron resonance.

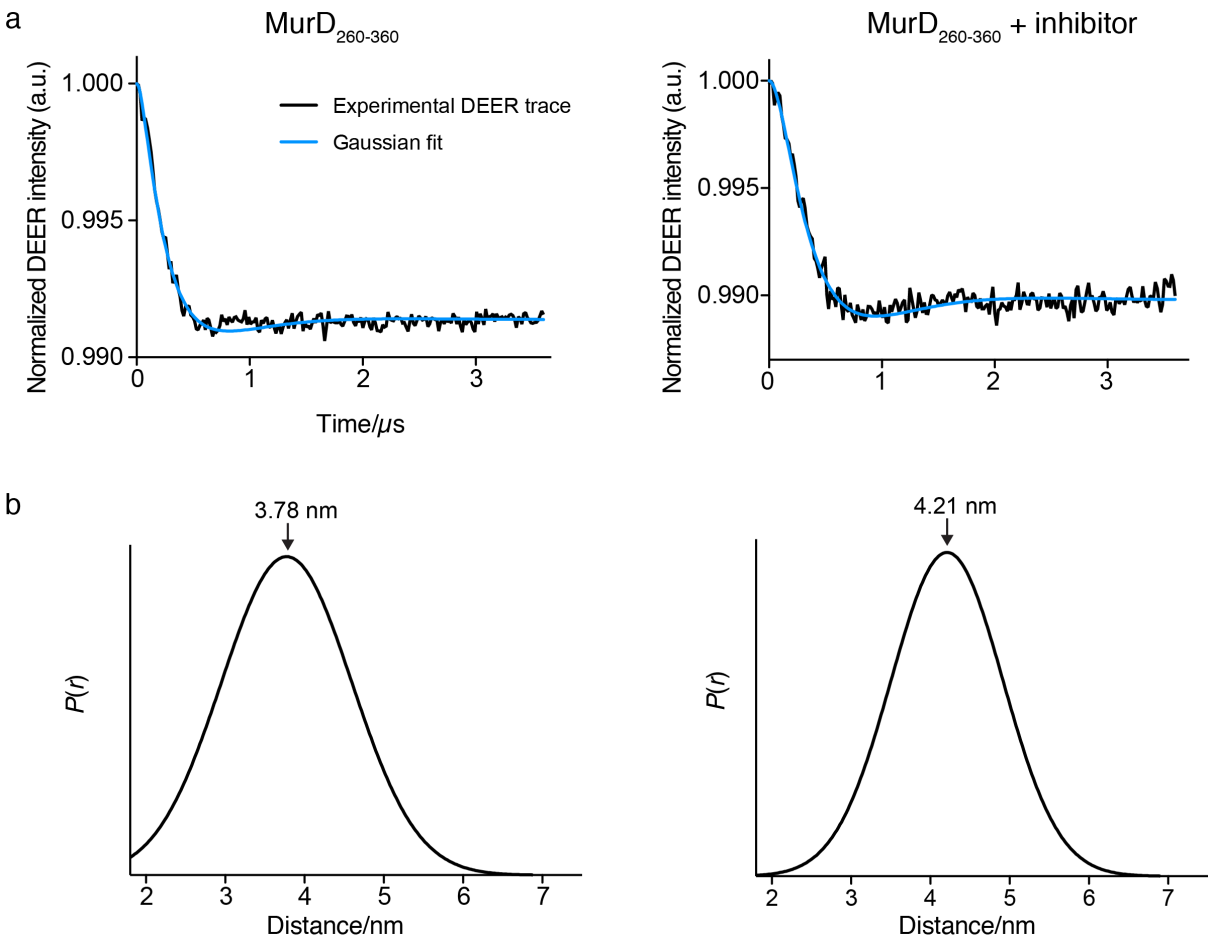

Figure S7 Single Gaussian fit of the DEER traces of $MurD_{260-360}$ in the absence and presence of the inhibitor. The DEER results shown in Figure 3 were fitted by single Gaussian. The results for $MurD_{260–360}$ in the absence (left panels) and presence (right panels) of the inhibitor are shown. (a) DEER traces after background removal along with the fits obtained with single Gaussian fitting. (b) Distance distribution obtained by the fit shown in (a). The standard deviations were estimated as 0.81 nm (left panel) and 0.70 nm (right panel). The data were analyzed using DeerAnalysis2016. DEER, double electron–electron resonance.

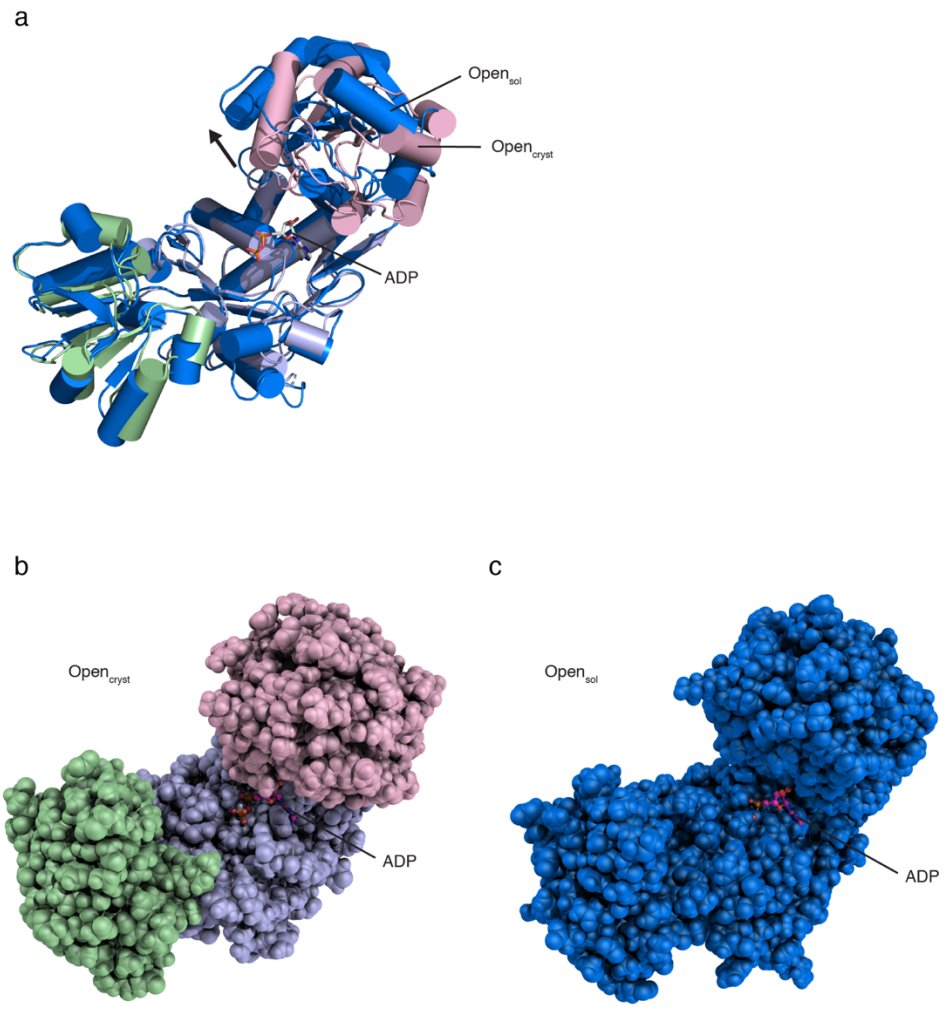

Figure S8 Comparison between the crystal structure and Open$_{sol}$ of MurD for ATP-binding site. (a) Superimposition of the crystal structure of MurD and the major conformational state of MurD in MD simulation. The coordinates are superimposed for domain 2. ADP, shown in sticks, is modeled based on the superimposition of the crystal structure of MurD in complex with ADP and UMA (3uag.pdb) for domain 2. (b), (c) The sphere representations of crystal structure (b) and the major MD conformation (c) of MurD. The ATP/ADP-binding site is wide open in the simulated structure. ADP, adenosine diphosphate; ATP, adenosine triphosphate; MD, molecular dynamics; UMA, UDP-*N*-acetylmuramoyl-L-alanine.